

Understanding the Physical and Material Dynamics of Multipulse Femtosecond Laser Interactions with Surfaces

Troy P. Anderson ^{*a}, Craig Zuhlke^a, Chris Wilson^a, Corey Kruse^b, Natale Ianno, Sidy Ndao^b,
George Gogos^b, Dennis Alexander^a

^aDept. of Electrical Engineering, University of Nebraska – Lincoln, 209N Scott Engineering Center, Lincoln, NE USA 68588; ^bDept. of Mechanical and Materials Engineering, University of Nebraska – Lincoln, 209N Scott Engineering Center, Lincoln, NE USA 68588

*troy.anderson@unl.edu

ABSTRACT

We describe the evolution of laser damage spots on bulk nickel generated by multipulse femtosecond laser irradiation with a 100 μm x 100 μm square flat-top beam profile as a function of the laser fluence and the number of pulses incident on the target. This large-area irradiation simulates conditions associated with the interaction of femtosecond laser pulses on a remote target. The larger area laser damage sites are characterized either by a series of self-organized surface structures with micro- and nanoscale features or a deep circular pit rather than a crater that mirrors the beam profile. Furthermore, the ablation rate of the deepest feature sharply increases above a laser fluence of 2 J/cm²; this increase is associated with the creation of a deep circular ablation pit generated during ablation with the first few pulses on the sample that continuously grows upon multipulse irradiation due to the focusing of incident laser energy into the pit by the sloped pit surfaces.

Keywords: Femtosecond Laser Ablation, Multipulse Ablation, Nickel

1. INTRODUCTION

The interaction of femtosecond lasers with materials is characterized by the deposition of laser energy into an electron plasma on a timescale shorter than the electron-phonon coupling time [1-4]. This ultrashort deposition time is termed athermal processing and allows the deposition of large amounts of energy into a well-defined region of the material without thermal effects during the lifetime of the pulse. For this reason, a common objective regarding the laser-matter interaction with femtosecond lasers has been focused on the ability to affect material properties or ablate material with high resolution and with minimal heat affected zone. Such research tends to minimize both the spot size on target as well as the number of laser shots incident on the target in order to achieve a high resolution [5-11]. However, a different regime of femtosecond laser interaction physics is gaining interest: the effects of multipulse femtosecond irradiation with a relatively large beam profile (tens to hundreds of microns). There are two driving forces behind research in this area: 1) the use of ultrashort lasers to interact with remote targets (e.g. through filaments) naturally requires large spot sizes and multiple laser shots to generate damage, 2) laser surface processing technology that utilize lasers to generate controlled surface morphologies benefit from large-area, multiple laser pulse interactions.

The primary interest in large-area multipulse femtosecond laser interactions to date has been in the field of surface processing. Specifically, it has been demonstrated that femtosecond laser damage with laser fluence values well above (>10X) the material ablation threshold is characterized by a series of self-organized surface structures with feature sizes on both the micro- and the nanoscale that develop over a large number of pulses [12-17]. These extreme laser conditions have been utilized to tailor various material surface properties including the fabrication of “black silicon” [18-22], near-blackbody metals [23,24], and superhydrophobic/superhydrophilic surfaces [25-29]. However, the physical mechanisms controlling the laser damage profile under large area multipulse conditions are still under investigation. Studies utilizing stop-motion SEM imaging have demonstrated that the laser fluence has a direct impact on both the physical interaction mechanisms and the resulting damage profiles; for example, the value of the laser fluence dictates whether surface structures rise above the original surface plane (Above Surface Growth Mounds) via fluid flow or sink below the original surface plane (Below Surface Growth Mounds) via preferential ablation mechanisms [13,30,31].

Of particular interest to this study and to the laser damage community, is the formation of catastrophic laser damage with large-area femtosecond laser beam profiles; this represents a unique laser ablation paradigm capable of producing deep ablation profiles and significant damage. The current paper characterizes the evolution of ablation pits on damage spots as a function of laser fluence and the number of pulses incident on the sample. Furthermore, the impact of the laser fluence on the ablation rate of the deepest pits and the ability to induce accelerated ablation in large pits is explored. The ability to generate deep laser damage sites using femtosecond lasers with large spot sizes and reasonable values of laser fluence is particularly applicable to long-distance laser damage, including laser filament-induced damage.

2. EXPERIMENT

The impact of multipulse femtosecond laser irradiation on the laser damage profile of a nickel substrate was investigated by fabricating a series of laser damage spots forming a grid in which the laser fluence and the number of laser shots incident on the sample were independently verified. This methodology enabled the analysis of trends associated with the fluence and the number of laser shots independently as well as provided a comprehensive picture of the interplay between these laser processing parameters. Specifically, the number of incident laser pulses ranged from 100 to 1000 and the laser fluence was varied from 1.1 J/cm^2 to 3.18 J/cm^2 . After illumination, each laser damage profile was analyzed via Scanning Electron Microscopy (SEM) and optical microscopy. Nickel was chosen as the substrate material due to the well-characterized physical characteristics and for compatibility with previous studies detailing the physical mechanisms of multipulse femtosecond laser surface processing.

2.1 Femtosecond Laser

The laser used for the study was a Spectra Physics Spitfire, Ti:Sapphire femtosecond laser system. The system is capable of producing 1 mJ, 50 fs pulses. In combination with a computer controlled shutter the repetition rate of the laser is adjustable from single pulses up to the maximum of 1 kHz. The pulse length and chirp were monitored using a Frequency Resolved Optical Gating (FROG) instrument from Positive Light (Model 8-02). The position of the sample with respect to the laser focal volume was controlled using computer-guided Melles Griot nanomotion translation stages with 3 axes of motion. A schematic of the experimental setup is provided in Figure 1.

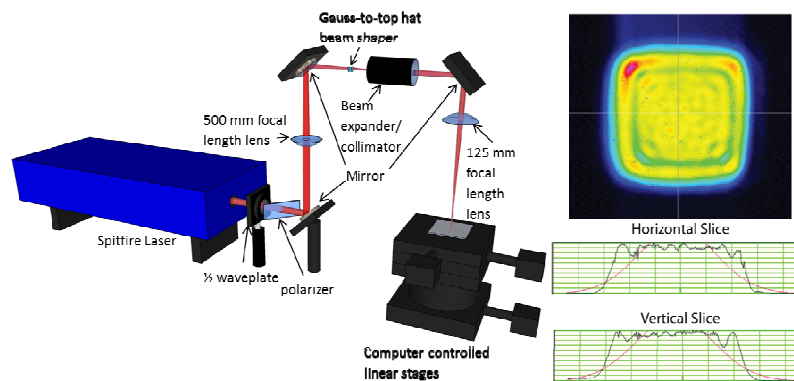


Figure 1: Configuration of the femtosecond laser and beam shaping optics (Image from Reference [13]).

The beam profile of the laser pulses incident on the sample was adjusted to be a square top-hat profile with dimensions of $100 \times 100 \mu\text{m}$. This flat beam profile was chosen over the standard Gaussian beam profile in order to isolate the impact of the laser fluence on the development of surface structures; a flat intensity beam minimizes fluence variations across the profile. The profile was generated using a Gaussian-to-Top Hat beam-shaping lens from Eksma Optics (GTH-4-2.2FA). In combination with a 125 mm focal length plano-convex lens, the beam shaper produced a square irradiance profile at the focal length of the 125 mm focal lens. The size of the square profile was adjustable according to Eq. 1. The beam expander/collimator in Figure 1 was used to adjust the NA of the system allowing for control of the square profile size. The 500 mm focal length lens was used to reduce the beam size from 5.2 cm at $1/e^2$ to the 4 cm at $1/e^2$ required for the beam shaper.

$$\text{Top Hat Size [mm]} = 4\mu\text{m}/\text{NA} \quad (1)$$

2.2 Surface Analysis

After processing, each irradiated spot was imaged using a Philips XL-30 Environmental Scanning Electron Microscope (SEM) manufactured by the FEI Company. The size and shape of surface features on the laser damage profile were characterized using morphological image analysis techniques to isolate the individual structures as well as the ablation pits and to provide relevant statistics on the size, shape, and eccentricity of both the structures and the pits. The analysis was performed using MATLABTM software and was implemented by: 1) performing a combination of morphological image processing of the grayscale image and thresholding to produce a binary image containing the outline of the structures of interest; and 2) statistical analysis of the structure outlines. These steps were performed twice: once to isolate and analyze the structures themselves and once to isolate and analyze the surrounding pits. An example surface morphology of a laser damage profile resulting from 300 laser pulses with a laser fluence of 1.58 J/cm^2 is shown in Figure 2. The original SEM image is shown in Figure 2(a) and the corresponding surface analysis in which surface structures are outlined in green and the pits are outlined in red is shown in Figure 2(b). Note that the analysis of the ablation pits is limited to the deeper features and not the valleys between each structure.

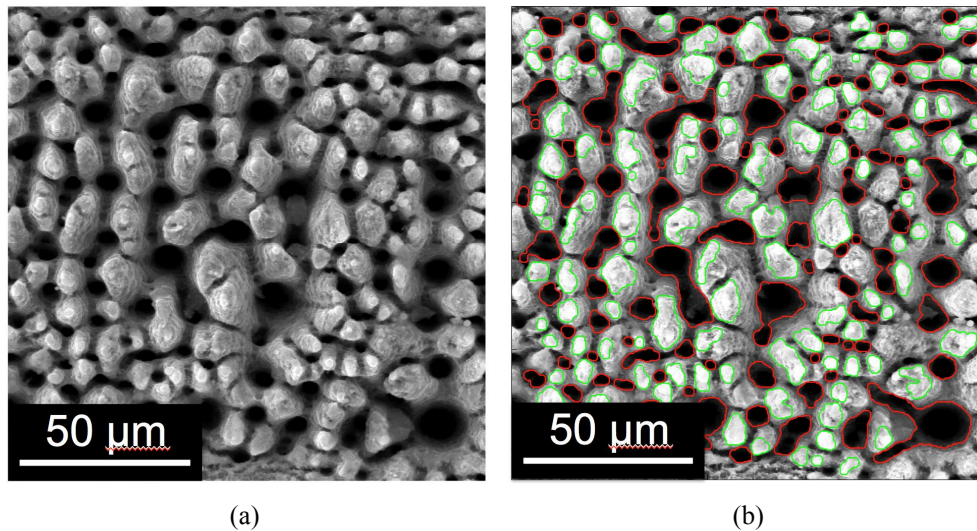


Figure 2: Output of image analysis algorithm to isolate and analyze surface structures on a nickel sample illuminated with 300 femtosecond laser pulses with a fluence of 1.58 J/cm^2 .

3. RESULTS AND DISCUSSION

Analysis of multishot laser damage profiles associated with a square flat-top beam profile with dimensions $100 \mu\text{m} \times 100 \mu\text{m}$ and fluence values significantly higher than the ablation threshold reveals that the laser damage cannot be fully described by the laser depth (or equivalently the ablation rate); rather, the laser damage profile is characterized by the generation of self-organized surface structures with properties that vary as a function of the laser fluence.

A representative sample of SEM images of the laser damage profiles as a function of the laser fluence and the number of pulses per shot is shown in Figure 3. Each square within the image represents an individual laser damage profile with a $100 \mu\text{m} \times 100 \mu\text{m}$ square flat-top beam profile.

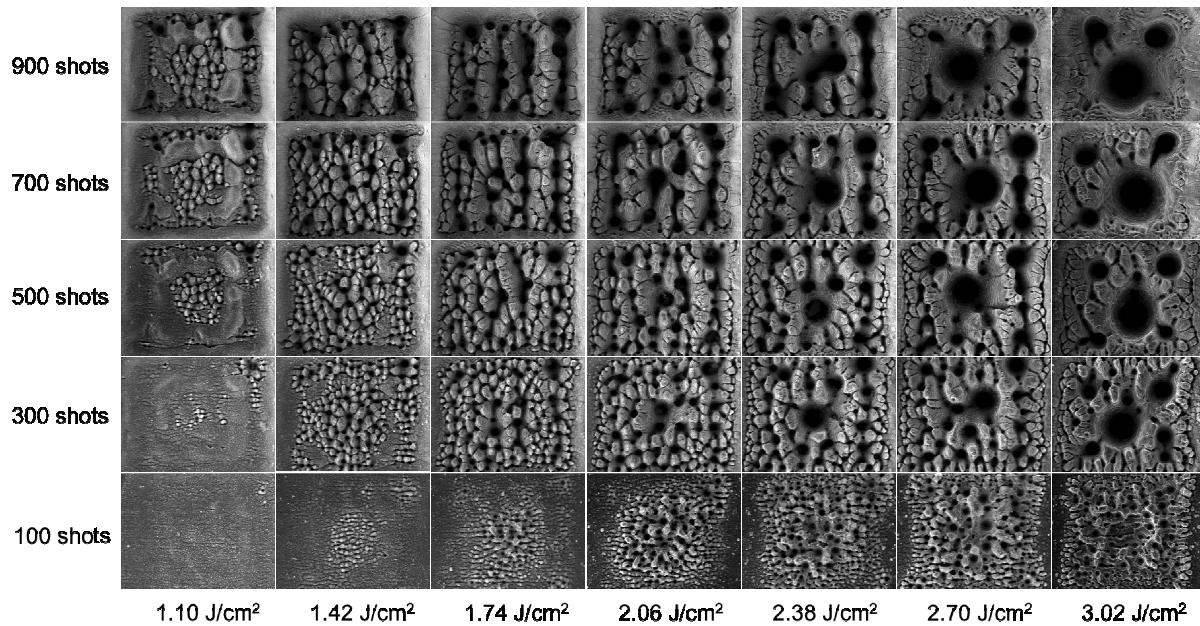


Figure 3: Representative sample of SEM images depicting the multishot femtosecond laser ablation profiles of a 100 μm x 100 μm square beam as a function of the laser fluence and the number of shots incident on the sample.

For low values of laser fluence and for low numbers of incident laser shots (e.g. 100 shots at 1.1 J/cm^2), the laser damage profile mirrors the laser beam profile. However, as both the laser fluence and the number of laser shots incident on the sample increase, a series of self-organized micron-scale features with diameters ranging from 5-20 μm appears, much less than the beam width. These self-organized surface structures have been previously reported in nickel [13,30] as well as other metals [32-35]. In between the self-organized features are a series of small ablation pits that vary in size and distribution according to the specific laser conditions. For 100 laser pulses incident on the sample, the size of the ablation pits does not change considerably within this range of fluence values. Similarly, little change is the pit size is observed for fluence values up to 1.42 J/cm^2 , regardless of the number of laser pulses incident on the sample. However, the size and distribution of ablation pits begins to change as both the laser fluence and the number of incident pulses is increased. In the most extreme cases considered, a deep circular ablation pit forms; under these conditions, the ablation profile has little resemblance to the square beam profile.

To further characterize the transition from laser damage profiles that mirror the beam profile to profiles characterized by deep pits, the maximum pit depth as a function of the laser fluence and number of incident pulses is plotted as in Figure 4. Each pixel represents the analysis of an individual laser damage profile (the images in Figure 3 are a subset of the larger series of analyzed laser damage profiles). The pixel color is related to the ablation depth with black representing no ablation and white representing the maximum measured ablated depth of 84 μm . The maximum pit depth increases with both laser fluence and the number of incident shots, closely following the trend of the pit diameter (values not shown but clear through visual inspection of Figure 3). Furthermore, this depth analysis indicates that the conditions for the formation of deep ablation pits on nickel are a laser fluence greater than $\sim 2 \text{ J}/\text{cm}^2$ and greater than 100 pulses incident on the sample. Once these conditions are met, further increasing either the number of laser shots or the laser fluence gives rise to a significant increase in the depth of the ablation pit. This trend is observed by noting the rapid rise in the ablation depth in the upper right section of the image for these laser parameters.

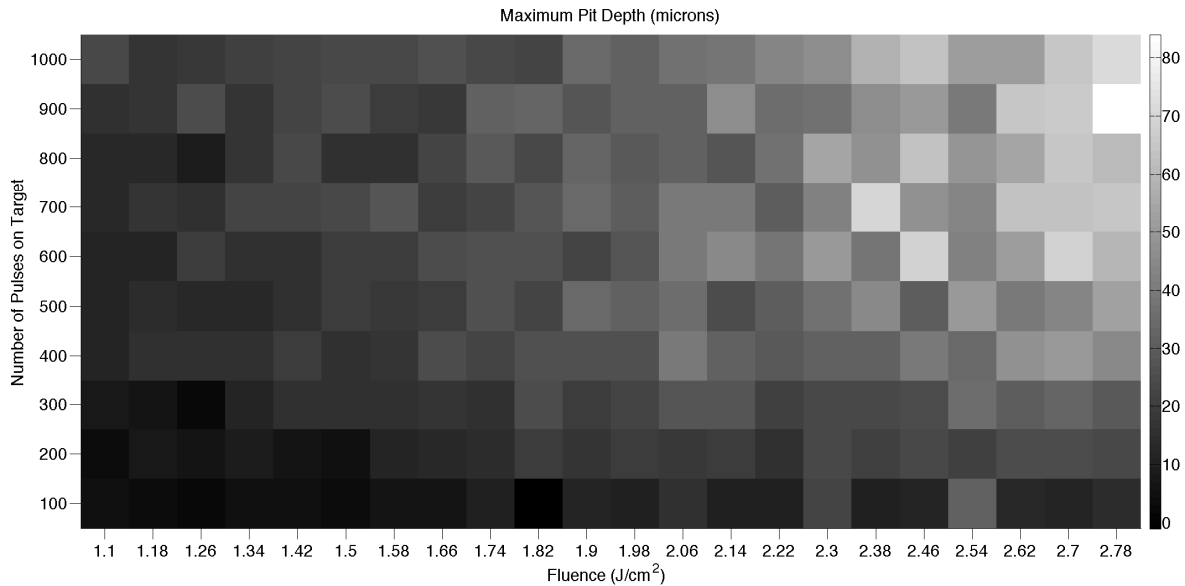


Figure 4: Maximum depth of the primary ablation pit as a function of the laser fluence and the number of laser pulses. Each pixel corresponds to the analysis of a single laser damage profile. The color of the pixel represents the ablation depth in units of microns.

The ablation rate of the primary pit for each laser damage site was calculated by dividing the pit depth of the primary pit by the number of laser shots. A plot of this maximum ablation rate as a function of fluence is shown in Figure 5. A clear discontinuity in the ablation rate exists at a laser fluence of 2 J/cm^2 . Specifically, the maximum ablation rate first increases slowly with fluence, ranging from $1.6 \text{ }\mu\text{m/shot}$ at 1.1 J/cm^2 to $1.96 \text{ }\mu\text{m/shot}$ at 1.98 J/cm^2 (approximate slope of 0.42 in this range). For laser fluence values larger than 2 J/cm^2 , the ablation rate increases significantly, reaching a value of $7.13 \text{ }\mu\text{m}$ per shot at 2.78 J/cm^2 (approximate slope of 5.4 in this range).

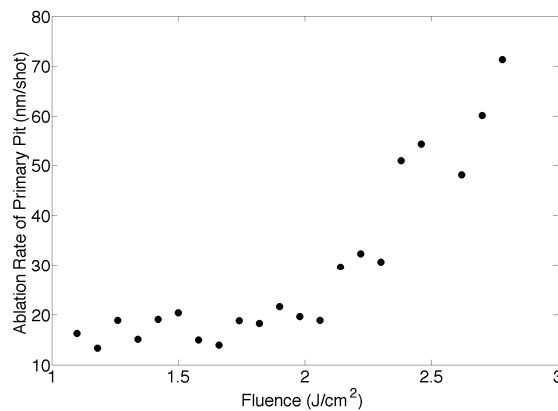


Figure 5: Ablation rate as a function of laser fluence for Nickel.

The discontinuity of the ablation rate at a laser fluence of 2 J/cm^2 coincides with a shift in the laser-matter interaction and the physical growth mechanisms of the self-organized features. Specifically, 2 J/cm^2 marks a transition in the response of the material to incident laser energy from the development of surface structures below the original surface plane via preferential ablation, and surface structures that rise above the original surface through fluid flow and redeposition of ablated material. The development of different classes of surface features via laser ablation of nickel as

well as the corresponding structural characteristics has been extensively studied in previous publications [13,30,31]. The transition between different classes of surface morphologies is clearly seen when inspecting not only the depth of the primary pit, but also the average pit depth. These parameters are plotted in Figure 6 as a function of the number of laser pulses for three representative values of laser fluence: 1.1 J/cm², 1.98 J/cm², and 2.78 J/cm², which correspond to the two extremes of the laser fluence range plotted in Figure 5 as well as the transition region.

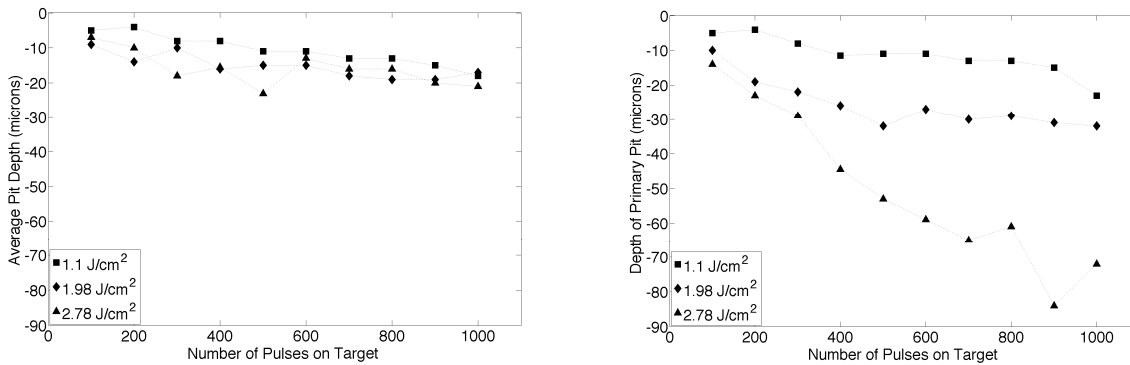


Figure 6: (a) Average pit depth, and (b) Maximum Pit Depth as a function of the number of pulses incident on the target for three values of the laser fluence.

The laser damage profiles fabricated at a laser fluence of 1.1 J/cm² are characterized by homogenous surface structures where the average and the maximum pit depth are roughly equal, which is consistent with the class of surface structures described as Below Surface Growth (BSG) Mounds that develop through surface-geometry-driven variations in the ablation rates on the sample. After a certain number of laser shots, the induced surface roughness contains micron-scale features that begin to scatter light and alter the distribution of laser energy on the sample in manner that further increases the structure size and thus self-organizes over a large number of laser pulses [13,15,36].

At a laser fluence of 1.98 J/cm², the structure homogeneity decreases and a maximum (primary) pit develops that is deeper than the average pit depth. As the laser fluence is increased, the induced temperature rise in the surface absorption region increases, which in turn amplifies the surface-geometry-driven variations in the ablation rates. Thermal loading effects due to the 100 μm spot size tends to generate a hot spot in the center of the beam profile and thus a primary ablation pit in the center of the profile. At 1.98 J/cm², this central pit is visible but not dominant. Further increasing the laser fluence (e.g. to 2.78 J/cm²) leads to accelerated ablation; once a central pit develops, the conical shape of the pit captures increasing amounts of the incident laser energy via multiple reflections, which causes the pit size and depth to grow with increasing pulse count. After sufficient growth, this pit dominates the entire laser damage profile. Depending on the desired application, this runaway condition leading to deep multipulse ablation can be utilized to generate a controlled series of deep pits on the surface or utilized to inflict significant laser damage on a remote target.

4. CONCLUSION

Laser damage profiles on a bulk nickel substrate generated by multipulse femtosecond laser ablation with a 100 μm x 100 μm beam diameter were characterized as a function of laser fluence and the number of pulses incident on the target. This characterization is critical to the understanding of laser damage mechanisms on remote targets using femtosecond laser systems. The laser fluence has a direct and significant impact on the nature of the laser damage site. Specifically, the laser damage profile is characterized by a series of self-organized surface structures that develop over hundreds of laser pulses. Thus, the laser damage sites cannot be sufficiently characterized by a simple ablation rate or ablation depth; rather the geometry of the resulting surface must be taken into account. Furthermore, increasing the laser fluence in a range from 1.1 J/cm² to 3.18 J/cm² results in a transition from laser damage sites that mirror the beam profile to sites characterized by a large ablation pit induced by surface-geometry-induced accelerated ablation. This transition is most concretely described by a discontinuity and rapid increase of the ablation rate above laser fluence of 2 J/cm². This multipulse, geometry-driven, deep ablation regime is a new paradigm of femtosecond laser damage that has potential applications to long-range interaction of femtosecond lasers with targets, including laser filament interactions.

REFERENCES

- [1] R. R. Gattass and E. Mazur, "Femtosecond laser micromachining in transparent materials," *Nature Photonics* **2**(4), 219–225, Nature Publishing Group (2008) [doi:10.1038/nphoton.2008.47].
- [2] B. Stuart, M. Feit, A. Rubenchik, B. Shore, and M. Perry, "Laser-Induced Damage in Dielectrics with Nanosecond to Subpicosecond Pulses," *Phys Rev Lett* **74**(12), 2248–2252 (1995).
- [3] S. K. Sundaram and E. Mazur, "Inducing and probing non-thermal transitions in semiconductors using femtosecond laser pulses," *Nat Mater* **1**(4), 217 (2002) [doi:doi:10.1038/nmat767].
- [4] S. Mao, F. Quere, S. Guizard, X. Mao, R. Russo, G. Petite, and P. Martin, "Dynamics of femtosecond laser interactions with dielectrics," *Appl. Phys. A* **79**, 1695–1709 (2004).
- [5] C. Momma, S. Nolte, B. N Chichkov, and A. Tünnermann, "Precise laser ablation with ultrashort pulses," *Applied Surface Science* **109**, 15–19, Elsevier (1997).
- [6] F. Korte, S. Adams, E. Egbert, C. Fallnich, A. Ostendorf, S. Nolte, M. Will, J.-P. Ruske, B. Chichkov, et al., "Sub-diffraction limited structuring of solid targets with femtosecond laser pulses," *Opt. Express* **7**(2), 41 (2000).
- [7] P. Gonzales, R. Bernath, J. Duncan, T. Olmstead, and M. Richardson, "Femtosecond ablation scaling for different materials," *Proceedings of SPIE* **5458**, 265–272 (2004).
- [8] S. Nolte, C. Momma, H. Jacobs, A. Tünnermann, B. N. Chichkov, B. Wellegehausen, and H. Welling, "Ablation of metals by ultrashort laser pulses," *JOSA B* **14**(10), 2716–2722, Optical Society of America (1997).
- [9] P. P. Pronko, S. K. Dutta, J. Squier, J. V. Rudd, D. Du, and G. Mourou, "Machining of sub-micron holes using a femtosecond laser at 800 nm," *Optics Communications* **114**(1), 106–110, Elsevier (1995).
- [10] L. Shah, J. Tawney, M. Richardson, and K. Richardson, "Femtosecond laser deep hole drilling of silicate glasses in air," *Applied Surface Science* **183**, 151–164 (2001).
- [11] P. Simon and J. Ihlemann, "Ablation of submicron structures on metals and semiconductors by femtosecond UV-laser pulses," *Applied Surface Science* **109**, 25–29, Elsevier (1997).
- [12] T. Her, R. Finlay, C. Wu, S. Deliwala, and E. Mazur, "Microstructuring of silicon with femtosecond laser pulses," *Applied Physics Letters* **73**(12), 1673–1675 (1998).
- [13] C. A. Zuhlke, T. P. Anderson, and D. R. Alexander, "Formation of multiscale surface structures on nickel via above surface growth and below surface growth mechanisms using femtosecond laser pulses," *Opt. Express* **21**(7), 8460–8473, Optical Society of America (2013) [doi:10.1364/OE.21.008460].
- [14] B. R. Tull, J. E. Carey, E. Mazur, J. P. McDonald, and S. M. Yalisove, "Silicon Surface Morphologies after Femtosecond Laser Irradiation," *Mrs Bull* **31**, 626–633 (2006).
- [15] B. K. Nayak and M. C. Gupta, "Ultrafast laser-induced self-organized conical micro/nano surface structures and their origin," *Optics and Lasers in Engineering* **48**(10), 966–973 (2010) [doi:10.1016/j.optlaseng.2010.05.009].
- [16] Z. Guo, S. Qu, S. Liu, and J.-H. Lee, "Periodic microstructures induced by interfered femtosecond laser pulses," presented at 5th International Symposium on Advanced Optical Manufacturing and Testing Technologies: Design, Manufacturing, and Testing of Micro- and Nano-Optical Devices and Systems, 2010, 76570K–76570K–7, SPIE [doi:10.1117/12.866233].
- [17] K. Kuršelis, R. Kiyan, and B. N. Chichkov, "Formation of corrugated and porous steel surfaces by femtosecond laser irradiation," *Applied Surface Science* **258**(22), 8845–8852 (2012) [doi:10.1016/j.apsusc.2012.05.102].
- [18] C. Wu, C. Crouch, L. Zhao, J. Carey, R. Younkin, J. Levinson, E. Mazur, R. Farrell, P. Gothoskar, et al., "Near-unity below-band-gap absorption by microstructured silicon," *Applied Physics Letters* **78**(13), 1850–1852 (2001).
- [19] R. Younkin, J. Carey, E. Mazur, J. Levinson, and C. Friend, "Infrared absorption by conical silicon microstructures made in a variety of background gases using femtosecond-laser pulses," *J. Appl. Phys.* **93**(5), 2626–2629 (2003) [doi:10.1063/1.1545159].
- [20] L. Ma, Y. Zhou, N. Jiang, X. Lu, J. Shao, W. Lu, J. Ge, X. Ding, and X. Hou, "Wide-band 'black silicon' based on porous silicon," *Applied Physics Letters* **88**(17), 171907 (2006) [doi:10.1063/1.2199593].
- [21] S. Koynov, M. S. Brandt, and M. Stutzmann, "Black nonreflecting silicon surfaces for solar cells," *Applied Physics Letters* **88**(20), 203107, American Institute of Physics (2006) [doi:10.1063/1.2204573].
- [22] L. Tsakalakos, J. Balch, J. Fronheiser, M.-Y. Shih, S. F. LeBoeuf, M. Pietrzykowski, P. J. Codella, B. A. Korevaar, O. Sulima, et al., "Strong broadband optical absorption in silicon nanowire films," *J Nanophotonics* **1**, 013552 (2007) [doi:10.1117/1.2768999].
- [23] A. Vorobyev and C. Guo, "Femtosecond laser blackening of metals," *Circuits and Systems, 2009. MWSCAS'09. 52nd IEEE International Midwest Symposium on*, 905–908 (2009).

- [24] A. Y. Vorobyev, A. N. Topkov, O. V. Gurin, V. A. Svich, and C. Guo, "Enhanced absorption of metals over ultrabroad electromagnetic spectrum," *Applied Physics Letters* **95**(12), 121106 (2009) [doi:10.1063/1.3227668].
- [25] C. Kruse, T. P. Anderson, C. Wilson, C. Zuhlke, D. R. Alexander, G. Gogos, and S. Ndao, "Extraordinary Shifts of the Leidenfrost Temperature from Multiscale Micro/Nanostructured Surfaces," *Langmuir* **29**(31), 9798–9806, American Chemical Society (2013) [doi:10.1021/la401936w].
- [26] E. Fadeeva, V. K. Truong, M. Stiesch, undefined author, R. J. Crawford, J. Wang, and E. P. Ivanova, "Bacterial Retention on Superhydrophobic Titanium Surfaces Fabricated by Femtosecond Laser Ablation," *Langmuir* **27**, 3012–3019 (2011).
- [27] E. Fadeeva, S. Schlie, J. Koch, A. Ngezahayo, and undefined author, "The hydrophobic properties of femtosecond laser fabricated spike structures and their effects on cell proliferation," *Phys. Status Solidi (a)* **206**(6), 1348–1351 (2009) [doi:10.1002/pssa.200881063].
- [28] A. Y. Vorobyev and C. Guo, "Laser turns silicon superwicking," *Opt. Express* **18**(7), 6455–6460, Optical Society of America (2010) [doi:10.1364/OE.18.006455].
- [29] D. Zhang, F. Chen, G. Fang, Q. Yang, D. Xie, G. Qiao, W. Li, J. Si, and X. Hou, "Wetting characteristics on hierarchical structures patterned by a femtosecond laser," *J Micromech Microeng* **20**(7), 075029, IOP Publishing (2010) [doi:10.1088/0960-1317/20/7/075029].
- [30] C. A. Zuhlke, T. P. Anderson, and D. R. Alexander, "Comparison of the structural and chemical composition of two unique micro/nanostructures produced by femtosecond laser interactions on nickel," *Applied Physics Letters* **103**(12), 121603–121603–5, AIP Publishing LLC (2013) [doi:10.1063/1.4821452].
- [31] C. A. Zuhlke, T. P. Anderson, and D. R. Alexander, "Fundamentals of layered nanoparticle covered pyramidal structures formed on nickel during femtosecond laser surface interactions," *Applied Surface Science* (2013) [doi:10.1016/j.apsusc.2013.07.002].
- [32] B. K. Nayak and M. C. Gupta, "Self-organized micro/nano structures in metal surfaces by ultrafast laser irradiation," *Optics and Lasers in Engineering* **48**(10), 940–949 (2010) [doi:10.1016/j.optlaseng.2010.04.010].
- [33] B. K. Nayak, M. C. Gupta, and K. W. Kolasinski, "Formation of nano-textured conical microstructures in titanium metal surface by femtosecond laser irradiation," *Appl. Phys. A* **90**(3), 399–402 (2007) [doi:10.1007/s00339-007-4349-2].
- [34] A. Y. Vorobyev and C. Guo, "Direct femtosecond laser surface nano/microstructuring and its applications," *Laser & Photon. Rev.*, n/a–n/a (2012) [doi:10.1002/lpor.201200017].
- [35] E. Stratakis, A. Ranella, and C. Fotakis, "Biomimetic micro/nanostructured functional surfaces for microfluidic and tissue engineering applications," *Biomicrofluidics* **5**(1), – (2011) [doi:10.1063/1.3553235].
- [36] T. Yong Hwang and C. Guo, "Polarization and angular effects of femtosecond laser-induced conical microstructures on Ni," *J. Appl. Phys.* **111**(8), 083518–083518–4, American Institute of Physics (2012) [doi:10.1063/1.4704394].